Journal Pre-proof

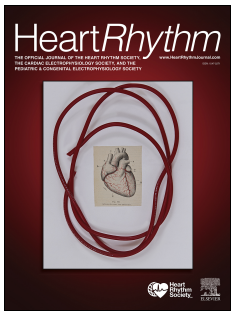

Cardiac stereotactic body radiotherapy to treat malignant ventricular arrhythmias directly affects the cardiomyocyte electrophysiology

Christine Mages, MD, Heike Gampp, Ann-Kathrin Rahm, MD, Juline Hackbarth, Julia Pfeiffer, Finn Petersenn, Xenia Kramp, Fatemeh Kermani, Juan Zhang, PhD, Daniel A. Pijnappels, PhD, Antoine A.F. de Vries, PhD, Katharina Seidensaal, MD, Bernhard Rhein, PhD, Jürgen Debus, MD, Nina D. Ullrich, PhD, Norbert Frey, MD, Dierk Thomas, MD, Patrick Lugenbiel, MD

PII: S1547-5271(24)02817-0

DOI: https://doi.org/10.1016/j.hrthm.2024.06.043

Reference: HRTHM 10579

To appear in: *Heart Rhythm*

Received Date: 19 May 2024

Revised Date: 21 June 2024

Accepted Date: 22 June 2024

Please cite this article as: Mages C, Gampp H, Rahm A-K, Hackbarth J, Pfeiffer J, Petersenn F, Kramp X, Kermani F, Zhang J, Pijnappels DA, de Vries AAF, Seidensaal K, Rhein B, Debus J, Ullrich ND, Frey N, Thomas D, Lugenbiel P, Cardiac stereotactic body radiotherapy to treat malignant ventricular arrhythmias directly affects the cardiomyocyte electrophysiology, *Heart Rhythm* (2024), doi: https://doi.org/10.1016/j.hrthm.2024.06.043.

Neonatal Rat Ventricular Cardiomyocytes

Irradiation
20 Gy Photon Radiation

Time Intervals of Analysis

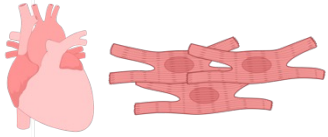

Overview 96h after Irradiation

Connexin 43

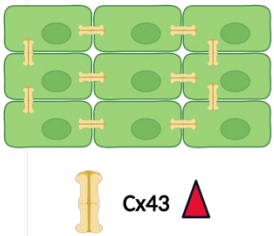

Action Potential

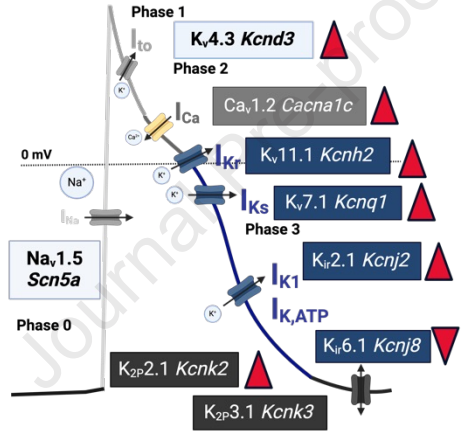

Calcium Handling

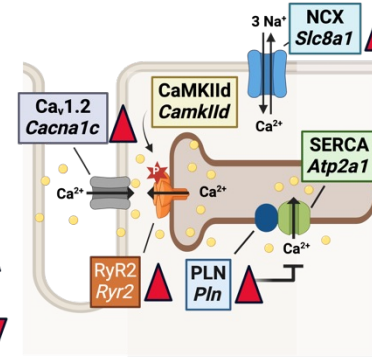

Functional Gap Junction Assessment

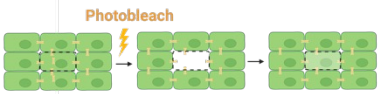

Fluorescence recovery

Optical Voltage Mapping and Video Analysis

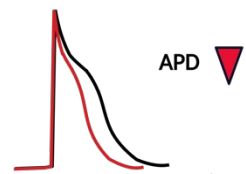

APD

Beating frequency

Conduction velocity

Calcium Imaging

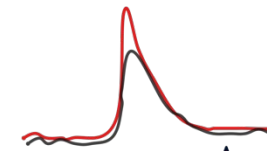

Calcium amplitude

Decay rate

Cardiac stereotactic body radiotherapy to treat malignant ventricular arrhythmias directly affects the cardiomyocyte electrophysiology

Running Title: Cardiac SBRT Directly Modulates Cardiomyocyte Electrophysiology

Authors: Christine Mages, MD [a,b,c,d#], Heike Gampp [a,b#], Ann-Kathrin Rahm, MD [a,b,c,d], Juline Hackbarth [a,b], Julia Pfeiffer [a,b], Finn Petersenn [a,b], Xenia Kramp [a,b], Fatemeh Kermani [e], Juan Zhang, PhD [f], Daniel A. Pijnappels, PhD [f], Antoine A. F de Vries, PhD[f], Katharina Seidensaal, MD [g,h], Bernhard Rhein, PhD [g,h], Jürgen Debus, MD [g,h], Nina D. Ullrich, PhD [c,e,i], Norbert Frey, MD [a,b,c,d], Dierk Thomas, MD [a,b,c], Patrick Lugenbiel, MD [a,b,c*]

Total Word Count: 5041

[a]Department of Cardiology, University Hospital Heidelberg, Heidelberg, Germany;

[b]Heidelberg Center for Heart Rhythm Disorders (HCR), University Hospital Heidelberg, Heidelberg, Germany;

[c]German Centre for Cardiovascular Research (DZHK), Partner site Heidelberg/Mannheim, University of Heidelberg, Heidelberg, Germany;

[d]Informatics4Life Consortium (Institute for Informatics Heidelberg), Heidelberg, Germany;

[e]Division of Cardiovascular Physiology, Institute of Physiology and Pathophysiology, Heidelberg, Germany;

fDepartment of Cardiology, Leiden University Medical Center, Leiden, the Netherlands

[g]Department of Radiation Oncology, Heidelberg University Hospital, Heidelberg, Germany;

[h]Heidelberg Institute of Radiation Oncology (HIRO), Heidelberg, Germany;

[i]Department of Physiology, University of Bern, Switzerland

# authors contributed equally

***Address for correspondence:** Patrick Lugenbiel, MD, FEHRA; Department of Cardiology, Heidelberg University, Im Neuenheimer Feld 410, 69120 Heidelberg, Germany; E-Mail: patrick.lugenbiel@med.uni-heidelberg.de

Funding: This work was supported in part by research grants from the University of Heidelberg, Faculty of Medicine (Postdoctoral Fellowships to P.L. and A.K.R.), from the German Cardiac Society (Fellowships to A.K.R. and P.L., Otto-Hess-Promotionsstipendium to H.G.), from the Elisabeth und Rudolf-Hirsch Stiftung für Medizinische Forschung (to A.K.R), from the Ernst und Berta Grimmke-Stiftung (to P.L.), from the Tschira-Foundation for InformaticsForLife to A.K.R. (research funding of C.M.), from the German Heart Foundation/German Foundation of Heart Research (Fellowship to A.K.R), from the German Internal Medicine Society (Clinician-Scientist-Program to A.K.R.), from the German Research Foundation (UL 466/2-1 to N.D.U.), and from the Joachim Siebeneicher Foundation (to D.T.).

Disclosures: C.M. acknowledges educational support from Biotronik and Johnson & Johnson, while A.K.R. acknowledges support from Boston Scientific, Johnson & Johnson, Abbott, and Medtronic. D.T. has received lecture fees/honoraria from various pharmaceutical and medical device companies, including Abbott, AstraZeneca, Bayer Vital, Boehringer Ingelheim Pharma, Bristol-Myers Squibb, Daiichi Sankyo, Johnson and Johnson Medical, Medtronic, Novartis, Pfizer Pharma, Sanofi-Aventis, and ZOLL CMS. P.L. has received lecture fees from Bayer Vital, Pfizer Pharma, and Bristol-Myers-Squibb, as well as educational support from Boston Scientific and fees/honoraria from Johnson & Johnson and Boston Scientific. The remaining authors have declared no relevant relationships.

Abstract

Background

Promising as a treatment option for life-threatening ventricular arrhythmias, cardiac stereotactic body radiotherapy (cSBRT) has demonstrated early antiarrhythmic effects within days of treatment. The mechanisms underlying the immediate and short-term antiarrhythmic effects are poorly understood.

Objectives

We hypothesize that cSBRT has a direct antiarrhythmic effect on cellular electrophysiology through reprogramming of ion channel and gap junction protein expression.

Methods

Following exposure to 20Gy of X-rays in a single fraction, neonatal rat ventricular cardiomyocytes (NRVCs) were analyzed 24 and 96h post-radiation to determine changes in conduction velocity, beating frequency, calcium transients, and action potential duration (APD) in both monolayers and single cells. Additionally, the expression of gap junction proteins, ion channels, and calcium handling proteins was evaluated at protein and mRNA levels.

Results

Following irradiation with 20Gy, NRVCs exhibited increased beat rate and conduction velocities 24 and 96h after treatment. mRNA and protein levels of ion channels were altered, with the most significant changes observed at the 96h-mark. Upregulation of *Cacna1c* ($Ca_v1.2$), *Kcnd3* ($K_v4.3$), *Kcnh2* ($K_v11.1$), *Kcnq1* ($K_v7.1$), *Kcnk2* ($K_{2P}2.1$), *Kcnj2* ($K_{ir}2.1$), and Gja1 (Cx43) was noted, along with improved gap junctional coupling. Calcium handling was affected, with increased *Ryr2* (RYR2) and *Slc8a1*

(NCX) expression and altered properties 96h post-treatment. Fibroblast and myofibroblast levels remained unchanged.

Conclusions

cSBRT modulates expression of various ion channels, calcium handling proteins, and gap-junction proteins. The described alterations in cellular electrophysiology may be the underlying cause of the immediate antiarrhythmic effects observed following cSBRT.

Keywords: radiation; ion channel; remodeling; neonatal rat cardiomyocytes; ventricular arrhythmia, sudden cardiac death.

Abbreviations list:

APD=Action potential Duration

cSBRT=Cardiac stereotactic body radiation therapy

CV=Conduction velocity

Cx43=Connexin 43

FDHM=Full duration at half maximum

hiPSC-CMs=Human induced pluripotent stem cell-derived cardiomyocytes

ICD=Implantable cardioverter-defibrillator

NRVCs=Neonatal rat ventricular cardiomyocytes

Rx=Irradiation

TTP=Time-to-peak

1. Introduction

Scar-related ventricular arrhythmias are a significant cause of morbidity and mortality in patients with impaired cardiac function and structural heart disease, often leading to sudden cardiac death.[1] Cardiac stereotactic body radiotherapy (cSBRT) for the treatment of ventricular tachycardia (VT) and ventricular fibrillation in patients with arrhythmic events has been an emerging technology within the last years and has shown promising effects in terms of immediate reduction of ventricular arrhythmias and ICD-interventions.[2] The latency of expected reduction of VT burden after cSBRT is of utmost importance due to the life-threatening character of ventricular arrhythmias. The antiarrhythmic effects of cardiac irradiation are thought to include the induction of scar homogenization and fibrosis. However, clinical studies consistently show that irradiation has an early antiarrhythmic effect within days of treatment, i.e. before the onset of fibrosis.[2–5] The molecular processes responsible for this initial antiarrhythmic effect have not yet been fully resolved.

The effect of immediate reduction of VT-burden was observed after 25Gy single-fraction photon irradiation (Rx).[2,4] At present, there is a lack of information regarding the minimum radiation dosage required to achieve antiarrhythmic effects. Radiation dose is mainly derived from preclinical studies, proposing electrophysiologic effects at or above 24Gy due to the induction of fibrosis.[4,6–8] This collectively suggests the potential for electrical remodeling independent of the onset of fibrosis.[2,4]

VTs are typically a result of myocardial re-entry occurring in regions with inhomogeneous scarring or at the edges of scars.[9] This type of re-entry is made possible due to the local slowing of electrical conduction caused by fibrosis as well as a decrease in gap junction coupling.[10]

Little is known about the radiation-dependent effects at the molecular level of cardiac electrophysiology; repeatedly, alterations of the cardiac conduction protein connexin 43 (Cx43) were described, but both up- and downregulation have been observed.[11–15] Recently an upregulation of Cx43 and the cardiac fast sodium channel $Na_v1.5$ was found six weeks after 25Gy whole heart irradiation in a mouse model with and without myocardial infarction causing an increase in cardiac conduction velocity (CV) reprogramming that was also achieved at lower Rx doses of 15 and 20Gy.[16] After 25Gy whole heart irradiation in rats, dynamic changes in the cardiac proteome, including proteins of the the cardiac conduction system were observed within one week.[15] Significant functional electrocardiographic changes were also observed in human induced pluripotent stem cell-derived cardiomyocytes (hiPSC-CMs) exposed to a single dose of X-rays of 20 to 50Gy.[17,18]

In the present study, we evaluated the mechanisms underlying the immediate antiarrhythmic effects of cSBRT. We hypothesized that radiation with less than 25Gy is sufficient to induce antiarrhythmic electrical remodeling.

2. Methods

Full experimental procedures and any associated references are available as Supplemental Material.

2.1 Ethics statement

Animal studies were conducted in accordance with the Guide for the Care and Use of Laboratory Animals as adopted and issued by the U.S. National Institutes of Health (NIH publication No. 85-23, revised 1985), and the current version of the German Law on the Protection of Animals was followed. This study conforms to Directive 2010/63/EU of the European Parliament.

2.2 Statistics

Statistical analyses were conducted using GraphPad Prism 6.0 software and OriginPro 2022 software. Data are presented as box and whisker plots with confidence intervals (CI), and the number of experiments (n) is indicated in each section. We used the unpaired, two-tailed Student's t-test or Mann-Whitney U test for unequal variances and the paired Student's t-test for comparisons within experimental groups across different time points. Significance was denoted as $*P<0.05$, $**P<0.01$, $***P<0.001$, $****P<0.0001$.

3. Results

3.1 Irradiated NRVC monolayers showed higher conduction velocity, shortened action potential duration, and increased beating frequency

We studied how Rx affects CV and action potential duration (APD) in NRVCs. At 24h after Rx, CV increased significantly (+30%, n=6; P<0.0001) (Fig. 1A). By 96h, CV was 1.6-fold higher than in controls (+165%, Ctrl n=5, Rx n=6, P=0.0014) (Fig. 1D). APD did not differ significantly at 24h but shortened significantly by 96h (APD_{50}: -52%, Ctrl n=5, Rx n=6; P<0.0001; APD_{90}: -50%, Ctrl n=5, Rx n=6; P<0.001) (Fig. 1E,F). Patch-clamp measurements at 24h showed APD_{90} shortening (-11%, n=27; P=0.026). No significant apoptosis was observed at 24 or 96h after Rx (Fig. S1), and cardiac troponin T (cTnt) mRNA expression remained stable (Fig S2). At 24h, cultures were mainly cardiomyocytes with ~4% fibroblasts; fibroblast proliferation number increased by 96h with no significant differences between irradiated and non-irradiated cultures (+28%, n=5; P=0.469) (Fig. S3). Irradiated cardiomyocytes showed an increase in beating frequency at 24h (+53%, n=6; P=0.002) and 96h (+59%, Ctrl n=8, Rx n=7; P<0.001) post-Rx (Fig. 1G), with greater variability compared to controls.

3.2 Ion channel remodeling after irradiation

We next examined radiation-induced electrophysiological remodeling at the molecular level and analysed differences in the expression of ion channel genes involved in the ventricular action potential by reverse transcription-quantitative polymerase chain reaction (RT-qPCR) analysis. At 24h after Rx, we found significant downregulation of the transcript levels of *Kcnq1*/K_v7.1 (n=6, P=0.036) and *Kcnj8*/K_{ir}6.1 (n=6, P=0.044) (Fig. 2A). Downregulation of *Kcnj8*/K_{ir}6.1 transcript persisted at 96h after Rx (n=6, P<0.0001). In contrast, the transcript levels of *Cacna1c*/Ca_v1.2 (n=6, P=0.023) and

the potassium channels *Kcnd3*/K_v4.3 (*n*=6, *P*=0.0005), *Kcnh2*/K_v11.1 (*n*=6, *P*<0.0001), *Kcnq1*/K_v7.1 (*n*=6, *P*<0.0001), *Kcnk2*/K_{2P}2.1 (*n*=6, *P*=0.032), and *Kcnj2*/K_{ir}2.1 (*n*=6, *P*=0.0001) were significantly upregulated at 96h after Rx compared to those in control cultures. We found no differences in the expression of *Scn5a*/Na_v1.5, *Kcne1*/MinK, and *Kcnk3*/K_{2P}3.1. Western blotting of samples harvested at 96h after Rx confirmed the RT-qPCR results at the protein level (Fig. 2B, C).

3.3 Irradiation improves intercellular coupling by upregulation of Cx43 and increased gap junction formation

To assess study effects of Rx on gap junctional coupling we assessed Cx43 expression (Fig. 3). At 24h after Rx, there were no significant changes in Cx43 mRNA (*P*=0.316) (Fig. 3A) or protein levels (*P*=0.890) (Fig. 3B, C). However, by 96h, both Cx43 mRNA (*P*<0.0001) and protein levels were upregulated (*P*<0.0001) (Fig. 3A, C). Immunostaining revealed a 45% increase in Cx43 expression at cell-to-cell contact zones in irradiated cardiomyocytes (*P*<0.0001) (Fig. 3D), indicating increased gap junction formation. Functional evaluation using fluorescence recovery after photobleaching showed significantly faster fluorescence recovery in irradiated cardiomyocytes (+24%, *P*=0.041), indicating enhanced functional gap junctions (Fig. 3E-G).

3.4 Irradiated neonatal rat ventricular cardiomyocytes showed altered calcium handling.

Calcium handling changes may affect CV and APD. Using IonOptix, we measured calcium transients (Fig. 4). At 24h, diastolic calcium increased in irradiated monolayers (+7%, *P*=0.0003) (Fig. 4B), together with a reduced time-to peak (TTP) and full duration at half maximum (FDHM) and time to peak (TTP; -26% and -23%,

respectively; *P*<0.0001) (Fig. 4B). At 96h, diastolic calcium remained elevated (+11%, *P*=0.0004), with further reductions in FDHM and TTP (-30% and -23%, respectively; *P*<0.0001) (Fig. 4D). Additionally, irradiated cardiomyocytes displayed increased calcium transient amplitudes and faster decay rates after 96h.

RT-qPCR and western blot analysis of genes involved in cardiac calcium handling (Fig. 5) showed an increase in PLN mRNA at 24h after Rx (*P*=0.012), which further increased by 96h (*P*<0.001), along with an increase in PLN protein (*P*=0.008). NCX mRNA and protein levels rose at 96h post-Rx as well as RyR2 mRNA (*P*=0.005). No significant changes were observed in CaMKIIδ and CaMKIIγ mRNA and protein levels at 24 or 96h after Rx.

3.5 Effects of irradiation on extracellular matrix

Next, we investigated the effect of irradiation on extracellular matrix formation and conversion of fibroblasts to paracrine active myofibroblasts in mixed cultures of cardiomyocytes and fibroblasts. The fibroblast-to-myofibroblast switch is accompanied by increases in the expression of α-smooth muscle actin (α-SMA) and the production of extracellular matrix components, a key event in connective tissue remodeling. As shown by western blotting, Rx did not significantly increase α-SMA or vimentin protein levels (Fig. 6).

4. Discussion

We investigated cSBRT's antiarrhythmic effects in NRVC cultures. A single Rx-dose of 20Gy led to an immediate rise in beat rate and CV, alongside significant APD shortening. We also observed changes in the expression of genes encoding ion channel and calcium handling proteins, notably at 96h post-Rx. These findings support the notion of an early antiarrhythmic impact preceding tissue damage. This study represents the first systematic exploration of cSBRT's immediate antiarrhythmic effects, highlighting the role of ion channels, gap junctional coupling, and calcium homeostasis in modifying cellular electrophysiology.

Irradiation affects electrophysiology in cardiomyocytes

In irradiated cardiomyocytes, there was a significant increase in beating frequency compared to the unirradiated group, possibly due to increased diastolic calcium levels. Mouse embryonic stem cells irradiated with 5Gy of γ-rays exhibited altered contractile properties and reduced beating frequency after differentiation into cardiomyocytes.[20] This discrepancy may be explained by the use of different experimental models, but could also suggest a dose-dependent effect.

Rx caused changes in the expression of cardiac ion channels directly affecting membrane excitability. Rx induced downregulation of *Kcnj8*/K_{ir}6.1 that persisted for 96h. *Cacna1c*/Ca_v1.2 and the potassium channels *Kcnd3*/K_v4.3, *Kcnh2*/K_v11.1, *Kcnk2*/K_{2P}2.1, and *Kcnj2*/K_{ir}2.1 showed significant upregulation at 96h after Rx. *Kcnq1*/K_v7.1 exhibited biphasic regulation with reduced expression at 24h and increased expression after 96h. Collectively, the changes in repolarizing potassium channel expression are suspected to shorten APD and to contribute to an increased CV. Exposure of iPSC-CMs to 20Gy did not lead to significant upregulation of *KCND3,*

KCNH2, SCN5A, CACNA1C or GJA1 after 7 days in contrast to Rx doses of 25 or 30Gy.[18] Interestingly, another research group reported a significant increase in $Na_v1.5$ density six weeks after whole heart irradiation of mice with 20Gy.[16] This disparity may be explained by compensatory mechanisms or dynamic changes that occur following irradiation, as indicated by large-scale proteomic analysis three and seven days after 2- and 25-Gy Rx.[15] These alterations resulted in APD shortening at 24h after Rx. This observation is consistent with our optical voltage mapping results, demonstrating increased CV and consistent APD shortening in irradiated NRVC monolayers.

Irradiation improves impulse propagation and conduction velocity

Our data showed upregulation of Cx43 and improved gap junction coupling in NRVCs at 96h after Rx, which can also in part explain the increased CV. Previous studies have reported that Cx43 expression is very sensitive to ionizing radiation in various cell lines.[21–24] Our study adds to this observation and confirms the hypothesis that the induced Cx43 proteins form functional channels. There are also contrary observations in the field, whose cause has not been clarified. Kim et al. showed a non-significant trend towards an increase in Cx43 mRNA following 20-Gy Rx of hiPSC-CMs.[18] Cha et al. even reported a reduction in Cx43 expression two and three weeks after irradiation with 20 to 50Gy by immunostaining of adult rat hearts.[17] The latter result is at odds with the observation that cardiac-specific postnatal loss of Cx43 slowed ventricular CV and increased the susceptibility to spontaneous ventricular arrhythmias and sudden cardiac death.[25] Moreover, other preclinical studeis also found increased cell-to-cell conduction via Cx43 upregulation upon 25Gy irradiation.[11–14] To our understanding, the inconsistencies in the field may arise from differences between animal models, type of radiation, and dose or timepoint of evaluation. Further studies are needed to address these different observations.

Calcium homeostasis and calcium handling proteins are affected by single dose irradiation

Regarding calcium handling proteins, significant upregulation of PLN, *Cacna1c*/$Ca_v1.2$, RYR2, and NCX mRNA and protein levels was detected after exposure of NRVCs to 20Gy. Kim et al.[15] reported an increase in RYR2 protein three days after exposure of adult rats to 25Gy, which is consistent with our findings. As mentioned previously, there are also reports indicating no significant changes in CACNA1C expression following 20-Gy irradiation,[18] a phenomenon that remains unexplained.

At the functional level, a variety of changes in the calcium transient properties were observed. We found persistently elevated radiation-dependent diastolic calcium levels. To our understanding this increase might arise from radiation-induced oxidative stress and reactive oxygen species (ROS) formation[26] leading to calcium leakage from the sarcoplasmic reticulum, as proposed previously.[27] However, we did not measure ROS formation in our model as this was not the scope of the present study. At 24 and 96h after Rx, we found faster kinetics of calcium transients as evidence by a reduction of TTP and FDHM. At 96h after Rx, calcium transients also showed increased amplitudes and faster decay rates. The increased amplitude may be associated with the observed upregulation of *Cacna1c*/$Ca_v1.2$ and RyR2. The faster decay rate might be related to the increased abundance of NCX. In a comprehensive study[27], Sag et al. assessed the acute (1h after irradiation) and chronic (one week after irradiation) effects of 20-Gy mediastinal photon radiation on calcium handling in murine cardiomyocytes. The investigation demonstrated an immediate elevation in calcium transient amplitudes post-irradiation, as opposed to a sustained reduction in the chronic phase. In contrast to our findings, the authors described an acute and chronic

322 irradiation-dependent activation of CaMKII due to increased oxidative stress.[27] In our
323 study, CaMKIIδ and CaMKIIγ levels were not affected by Rx. Also, while we found an
324 increase in Slc8a1 (NCX) expression and no change in Atp2a1 (SERCA) mRNA (Fig.
325 5) after Rx, in the study by Sag et al. NCX remained unchanged and SERCA2a
326 expression was decreased on week after Rx. We focused on the short-term effects up
327 to 96h post-Rx, leaving uncertainty regarding the normalization or exacerbation of
328 expression differences over time. However, both studies highlight the influence of
329 ionizing radiation on cardiac calcium handling, urging further research to grasp its
330 implications for antiarrhythmic effects.

331 **Significance for antiarrhythmic therapy**

332 In most heart diseases, re-entry mechanisms are based on remodeling processes
333 causing (local) conduction slowing.[28] Our data support early antiarrhythmic effects
334 through reprogramming of ion channels causing an increase in CV and APD
335 shortening in irradiated cardiomyocytes. These results are consistent with a study of
336 Anyukhovsky et al., which showed antiarrhythmic effects of improving the conduction
337 in slow conducting arrhythmogenic mouse tissue by Scn4a ($Na_v1.4$) or Gjb1 (connexin
338 32) gene transfer.[29] Shortening of the effective refractory period of the targeted
339 myocardium could lead to enhanced local conduction[30] and consequently, the re-entry
340 phenomenon would decrease through an electrical homogenization. As a therapeutic
341 approach, this could already demonstrate strong antiarrhythmic effects.[31,32] The
342 described effects of abolishing inhomogeneities and delayed conduction properties
343 within the scar, partially achieved through altered ion channel expressions and
344 improved gap junctional coupling, may represent a potentially effective antiarrhythmic
345 concept in the treatment of ventricular tachycardias in patients with scar-related
346 mechanisms. These effects occur independently of the formation of fibrous scars,

suggesting that these electrical changes can already be effectively observed at lower radiation doses. Further work in disease models will be essential to understand whether the response of the diseased myocardium is similar to that of healthy tissue.

Although the antiarrhythmic mechanisms of Rx remain to be determined, several studies showed early myocardial effects in a dose-dependent manner.[15–18] A persistent observation is that 20Gy is sufficient to achieve electrophysiological remodeling, although it remains unclear if those effects are long-lasting as suggested by our data. The currently used dose of 25Gy in patients was initially chosen to imitate the effects seen after radiofrequency ablation. Currently, ~81% of the patients receiving SBRT suffer from mild adverse effects[2,4], which highlights the importance of improving its safety through dose reduction. The reported data give a mechanistic insight into fast antiarrhythmic changes and underline the option for dose reduction without loss of efficacy. Initial clinical reports support effective antiarrhythmic treatment with a radiation dose even below 20Gy.[33]

Potential limitations and future directions

This study has several noteworthy limitations. We chose not to inhibit fibroblasts to better mimic the extracellular environment, which could impact the results as fibroblasts influence cardiomyocyte electrophysiology through heterocellular coupling. Neonatal cardiomyocytes were selected for patch-clamp investigations, with the present work focusing on a descriptive analysis of electrophysiological properties within a maximum of 96h post-irradiation. Further studies in a disease model are needed to enable the examination of adult cells over a longer observation period. Our model does not replicate diseased hearts, which significantly affects the causal interpretation of the results. Additionally, we used photon irradiation, but other

energies like protons or heavy ions may yield different effects and warrant investigation.[34,35]

5. Conclusion

Our results indicate an association of acute irradiation effects and electrophysiological remodeling in cardiomyocytes. Changes of cellular ion channel expression, calcium homeostasis and cell-cell-propagation lead to electrophysiological changes. Although the final mechanism causing antiarrhythmic changes remains to be discovered, these results reveal new insight into acute antiarrhythmic effects of cSBRT therapy on cardiomyocytes .

6. Acknowledgement

We declare that no artificial intelligence (AI) was used in preparation of the present manuscript.

We gratefully acknowledge the excellent technical assistance of Axel Schöffel, Teresa Caspari, Patrizia Lo Vetere, Nicole Westerhorstmann and Miriam Baier.

7. References

1. Zeppenfeld K, Tfelt-Hansen J, de Riva M, et al.: 2022 ESC Guidelines for the management of patients with ventricular arrhythmias and the prevention of sudden cardiac death: Developed by the task force for the management of patients with ventricular arrhythmias and the prevention of sudden cardiac death of the European Society of Cardiology (ESC) Endorsed by the Association for European Paediatric and Congenital Cardiology (AEPC). European Heart Journal 2022; 43:3997–4126.

2. Kovacs B, Mayinger M, Schindler M, Steffel J, Andratschke N, Saguner AM: Stereotactic radioablation of ventricular arrhythmias in patients with structural heart disease - A systematic review. Radiother Oncol 2021; 162:132–139.

3. Ninni S, Gallot-Lavallée T, Klein C, et al.: Stereotactic Radioablation for Ventricular Tachycardia in the Setting of Electrical Storm. Circ Arrhythm Electrophysiol 2022; 15:e010955.

4. van der Ree MH, Blanck O, Limpens J, et al.: Cardiac radioablation—A systematic review. Heart Rhythm Elsevier, 2020; 17:1381–1392.

5. Robinson CG, Samson, Moore, et al.: Phase I/II Trial of Electrophysiology-Guided Noninvasive Cardiac Radioablation for Ventricular Tachycardia. Circulation American Heart Association, 2018; 139:313–321.

6. Blanck O, Bode F, Gebhard M, et al.: Dose-escalation study for cardiac radiosurgery in a porcine model. Int J Radiat Oncol Biol Phys 2014; 89:590–598.

7. Chang JH, Cha M-J, Seo J-W, et al.: Feasibility study on stereotactic radiotherapy for total pulmonary vein isolation in a canine model. Sci Rep 2021; 11:12369.

8. Lehmann HI, Richter D, Prokesch H, et al.: Atrioventricular node ablation in Langendorff-perfused porcine hearts using carbon ion particle therapy: methods and an in vivo feasibility investigation for catheter-free ablation of cardiac arrhythmias. Circ Arrhythm Electrophysiol 2015; 8:429–438.

9. de Chillou C, Lacroix D, Klug D, et al.: Isthmus characteristics of reentrant ventricular tachycardia after myocardial infarction. Circulation 2002; 105:726–731.

10. de Bakker JM, van Capelle FJ, Janse MJ, et al.: Slow conduction in the infarcted human heart. “Zigzag” course of activation. Circulation 1993; 88:915–926.

11. Amino M, Yoshioka K, Tanabe T, et al.: Heavy ion radiation up-regulates Cx43 and ameliorates arrhythmogenic substrates in hearts after myocardial infarction. Cardiovasc Res Oxford Academic, 2006; 72:412–421.

12. Amino M, Yoshioka K, Fujibayashi D, et al.: Year-long upregulation of connexin43 in rabbit hearts by heavy ion irradiation. Am J Physiol Heart Circ Physiol 2010; 298:H1014-1021.

13. Viczenczova C, Szeiffova Bacova B, Egan Benova T, et al.: Myocardial connexin-43 and PKC signalling are involved in adaptation of the heart to irradiation-induced injury: Implication of miR-1 and miR-21. Gen Physiol Biophys 2016; 35:215–222.

14. Viczenczova C, Kura B, Egan Benova T, et al.: Irradiation-Induced Cardiac Connexin-43 and miR-21 Responses Are Hampered by Treatment with Atorvastatin and Aspirin. International Journal of Molecular Sciences Multidisciplinary Digital Publishing Institute, 2018; 19:1128.

15. Kim BH, Jung JW, Han D, Cha M-J, Chang JH: One-Week Dynamic Changes in Cardiac Proteomes After Cardiac Radioablation in Experimental Rat Model. Front Cardiovasc Med 2022; 9:898222.

16. Zhang DM, Navara R, Yin T, et al.: Cardiac radiotherapy induces electrical conduction reprogramming in the absence of transmural fibrosis. Nat Commun 2021; 12:5558.

17. Cha M-J, Seo J-W, Kim HJ, et al.: Early Changes in Rat Heart After High-Dose Irradiation: Implications for Antiarrhythmic Effects of Cardiac Radioablation. J Am Heart Assoc 2021; 10:e019072.

18. Kim JS, Choi SW, Park Y-G, et al.: Impact of High-Dose Irradiation on Human iPSC-Derived Cardiomyocytes Using Multi-Electrode Arrays: Implications for the Antiarrhythmic Effects of Cardiac Radioablation. Int J Mol Sci 2021; 23:351.

19. Grune T, Ott C, Häseli S, Höhn A, Jung T: The “MYOCYTER” – Convert cellular and cardiac contractions into numbers with ImageJ. Sci Rep Nature Publishing Group, 2019; 9:15112.

20. Rebuzzini P, Fassina L, Mulas F, et al.: Mouse embryonic stem cells irradiated with γ-rays differentiate into cardiomyocytes but with altered contractile properties. Mutat Res 2013; 756:37–45.

21. Sottas V, Wahl C-M, Trache MC, et al.: Improving electrical properties of iPSC-cardiomyocytes by enhancing Cx43 expression. Journal of Molecular and Cellular Cardiology 2018; 120:31–41.

22. Glover D, Little JB, Lavin MF, Gueven N: Low dose ionizing radiation-induced activation of connexin 43 expression. International Journal of Radiation Biology Taylor & Francis, 2003; 79:955–964.

23. Banaz-Yaşar F, Tischka R, Iliakis G, Winterhager E, Gellhaus A: Cell Line Specific Modulation of Connexin43 Expression after Exposure to Ionizing Radiation. Cell Communication & Adhesion Taylor & Francis, 2005; 12:249–259.

24. Azzam EI, de Toledo SM, Little JB: Expression of CONNEXIN43 is highly sensitive to ionizing radiation and other environmental stresses. Cancer Res 2003; 63:7128–7135.

25. Gutstein DE, Morley GE, Tamaddon H, et al.: Conduction slowing and sudden arrhythmic death in mice with cardiac-restricted inactivation of connexin43. Circ Res 2001; 88:333–339.

26. Kim W, Lee S, Seo D, et al.: Cellular Stress Responses in Radiotherapy. Cells Multidisciplinary Digital Publishing Institute, 2019; 8:1105.

27. Sag CM, Wolff HA, Neumann K, et al.: Ionizing radiation regulates cardiac Ca handling via increased ROS and activated CaMKII. Basic Res Cardiol 2013; 108:385.

28. Holmes JW, Laksman Z, Gepstein L: Making better scar: Emerging approaches for modifying mechanical and electrical properties following infarction and ablation. Progress in Biophysics and Molecular Biology 2016; 120:134–148.

29. Anyukhovsky EP, Sosunov EA, Kryukova YN, et al.: Expression of skeletal muscle sodium channel (Nav1.4) or connexin32 prevents reperfusion arrhythmias in murine heart. Cardiovasc Res 2011; 89:41–50.

30. Roell W, Lewalter T, Sasse P, et al.: Engraftment of connexin 43-expressing cells prevents post-infarct arrhythmia. Nature 2007; 450:819–824.

31. Greener ID, Sasano T, Wan X, et al.: Connexin43 gene transfer reduces ventricular tachycardia susceptibility after myocardial infarction. J Am Coll Cardiol 2012; 60:1103–1110.

32. Lau DH, Clausen C, Sosunov EA, et al.: Epicardial border zone overexpression of skeletal muscle sodium channel SkM1 normalizes activation, preserves conduction, and suppresses ventricular arrhythmia: an in silico, in vivo, in vitro study. Circulation 2009; 119:19–27.

33. Huang S-H, Wu Y-W, Shueng P-W, et al.: Case report: Stereotactic body radiation therapy with 12 Gy for silencing refractory ventricular tachycardia. Front Cardiovasc Med 2022; 9:973105.

34. Takami M, Hara T, Okimoto T, et al.: Electrophysiological and Pathological Impact of Medium-Dose External Carbon Ion and Proton Beam Radiation on the Left Ventricle in an Animal Model. J Am Heart Assoc 2021; 10:e019687.

35. Rapp F, Simoniello P, Wiedemann J, et al.: Biological Cardiac Tissue Effects of High-Energy Heavy Ions – Investigation for Myocardial Ablation. Scientific Reports Nature Publishing Group, 2019; 9:5000.

8. Figures

Figure 1

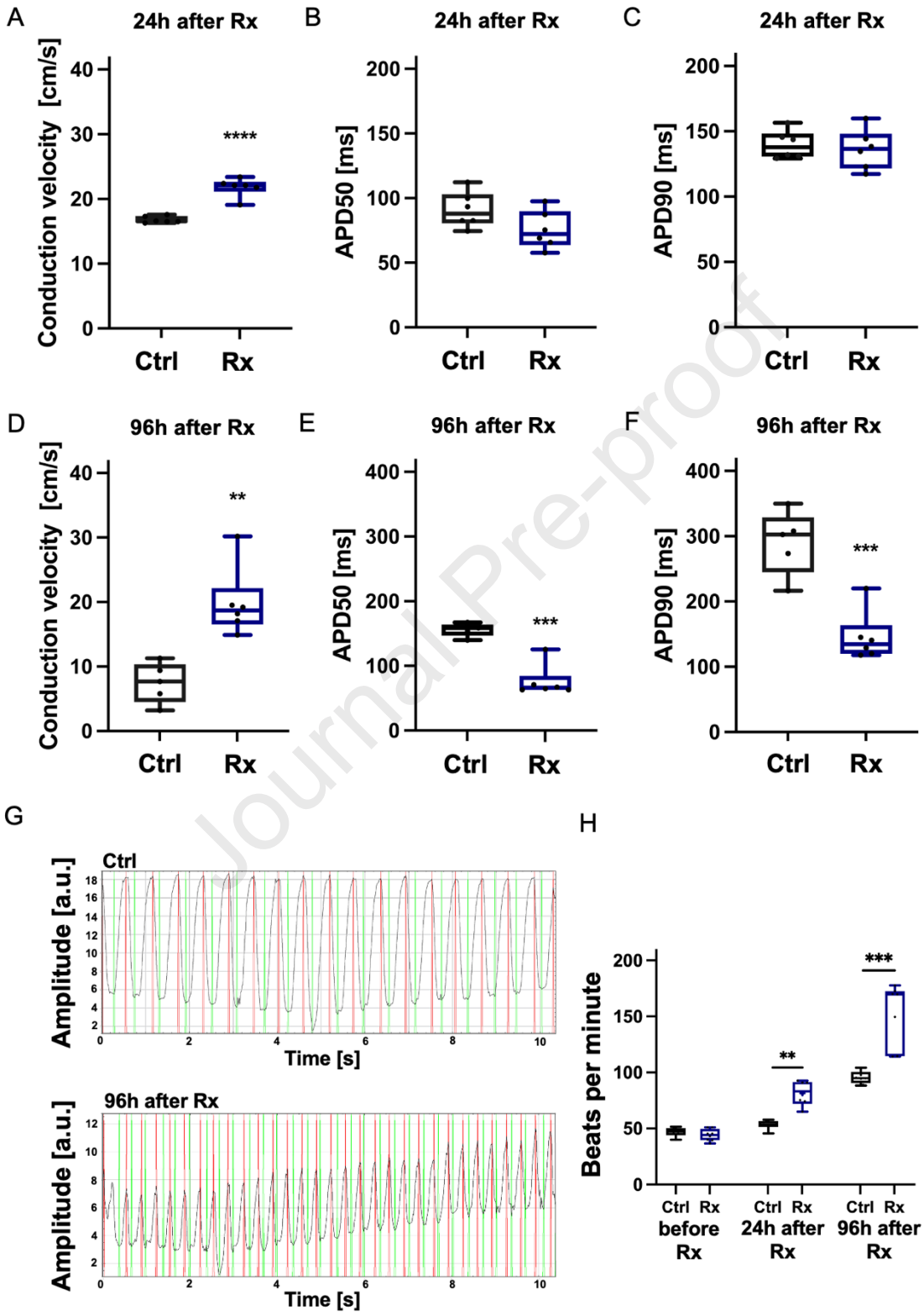

Figure 2

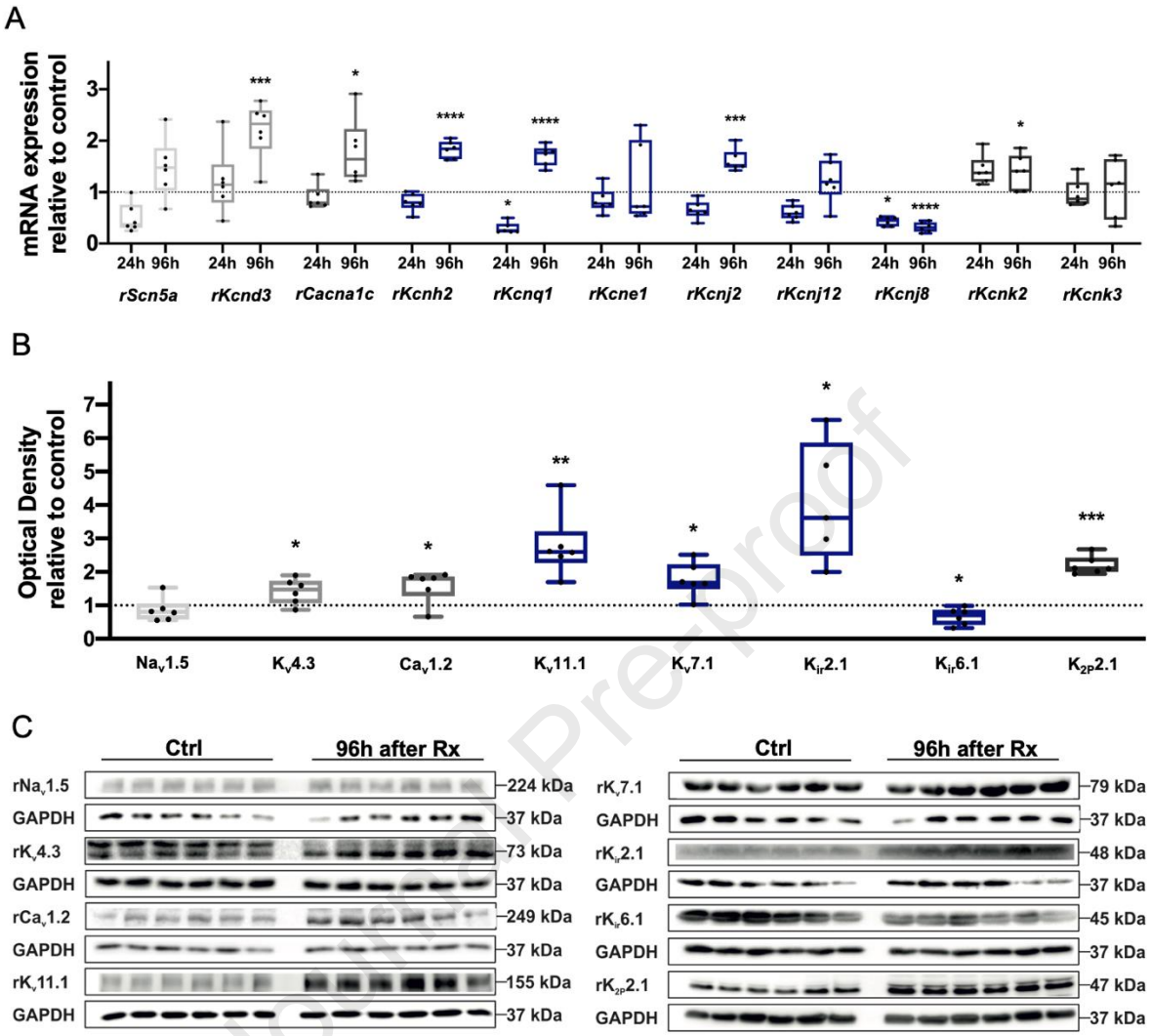

509 **Figure 3**

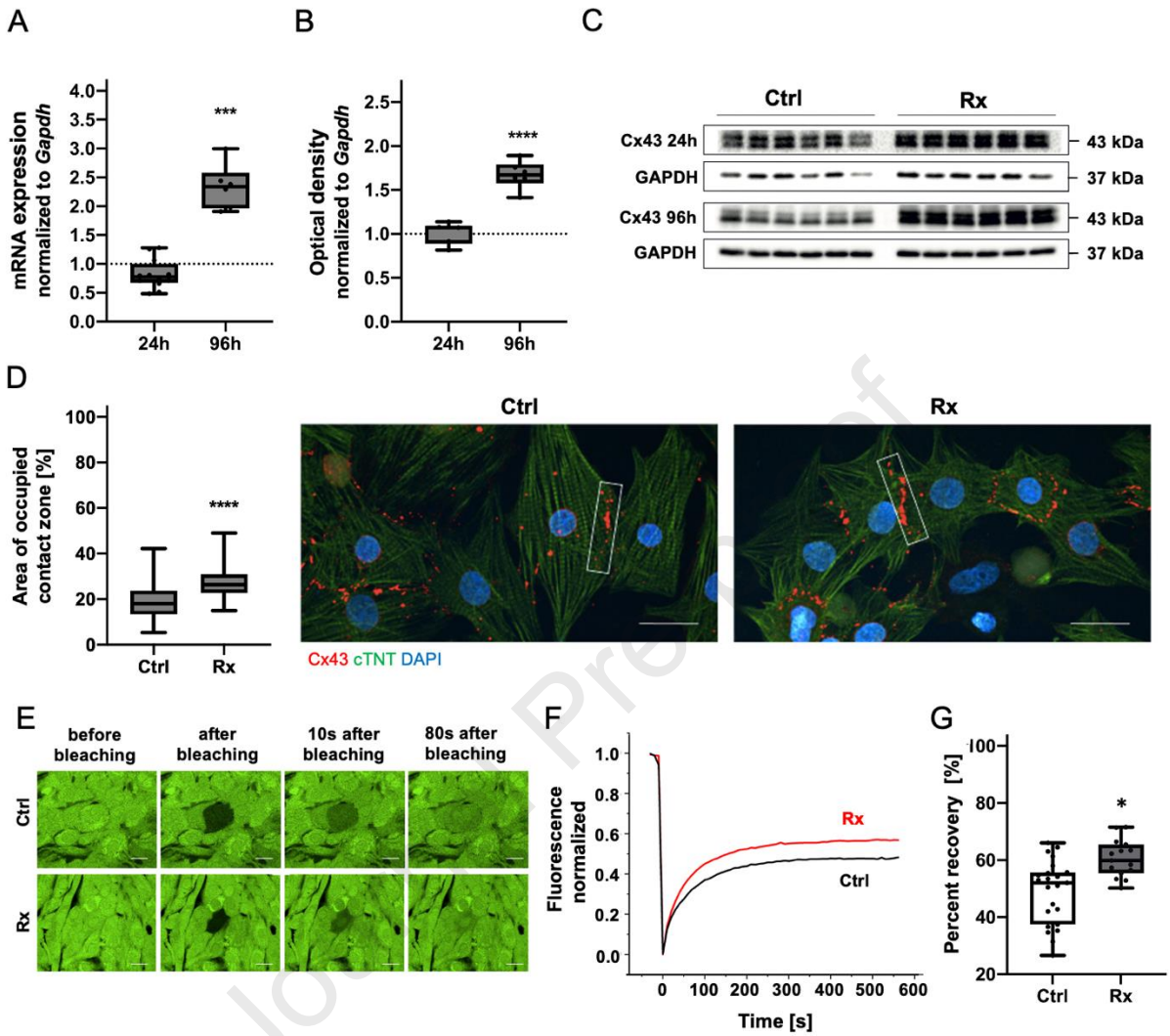

510

511

512

513

514

515

516

517 **Figure 4**

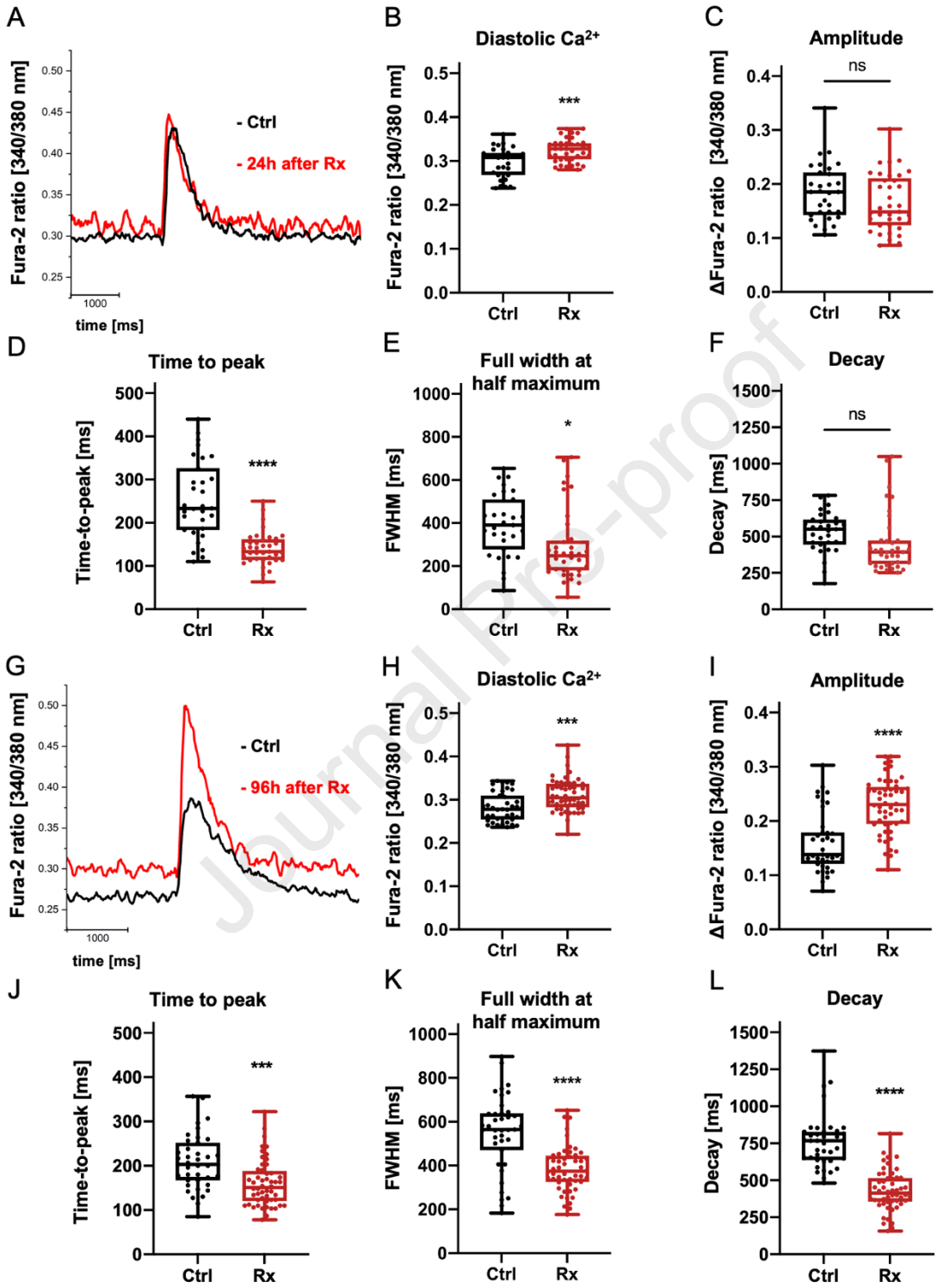

518

519

520 **Figure 5**

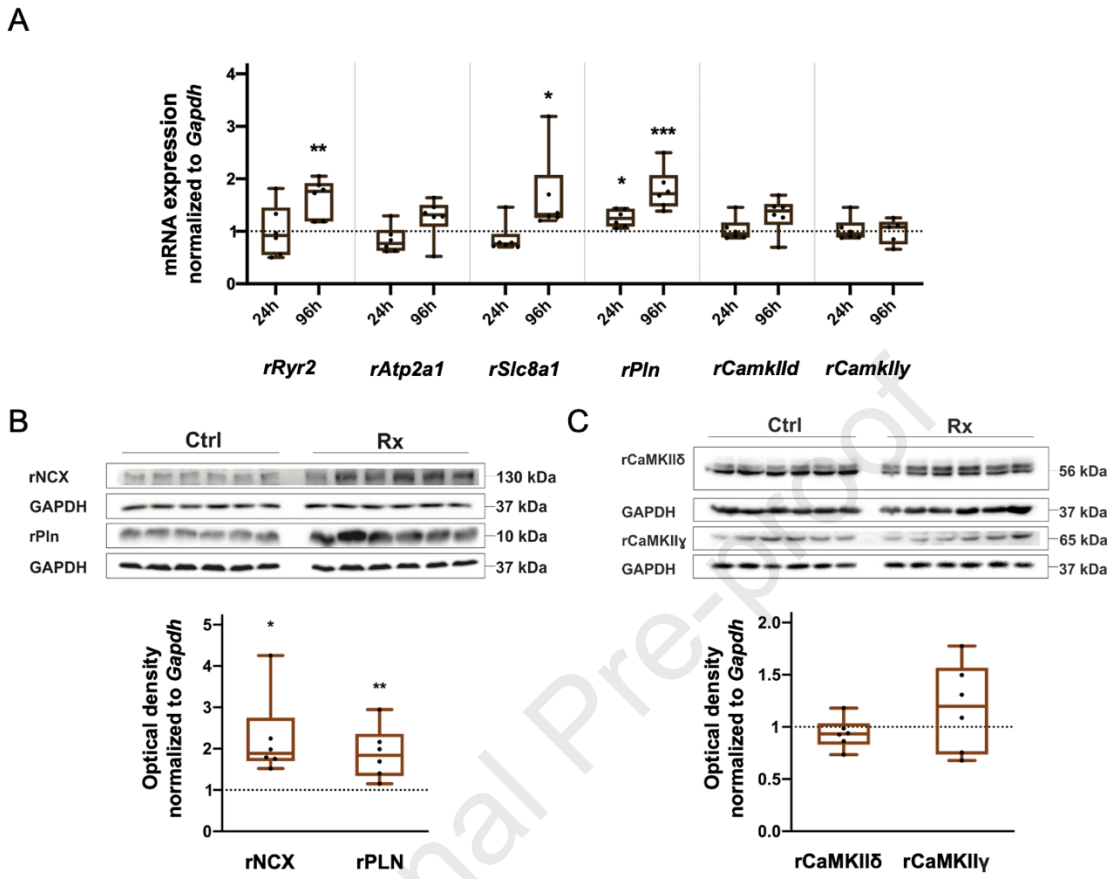

521

522

523

524

525

526

527

528

529

530 **Figure 6**

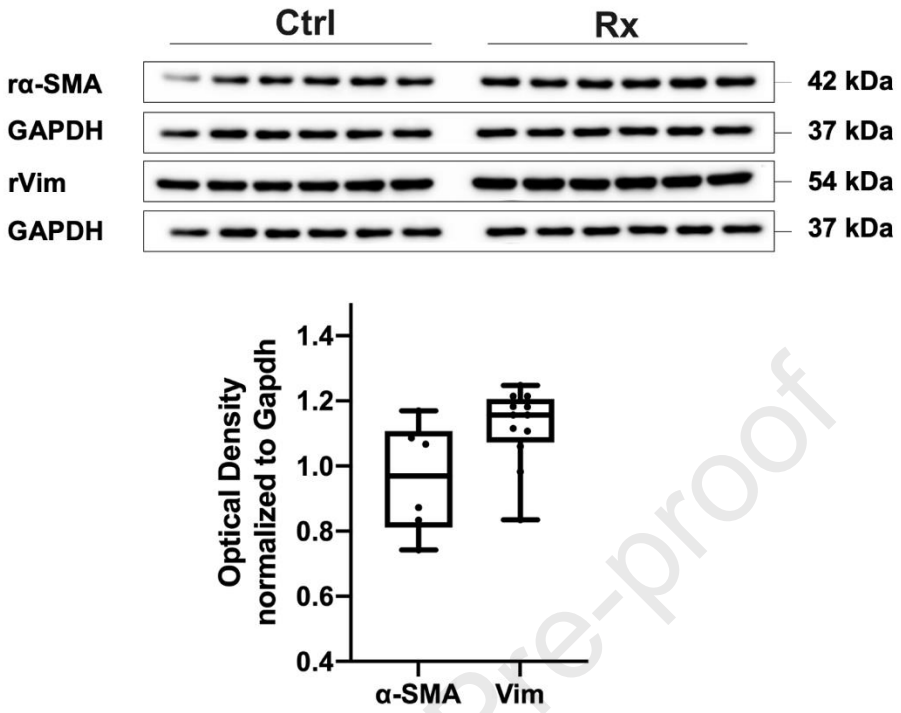

531

532

9. Figure legends

Graphical abstract: Overview of methods and major findings affecting the cellular electrophysiology 96h after 20Gy photon irradiation.

Fig.1: Irradiated NRVC monolayers showed significantly increased conduction velocity and increased beating frequency. A-F: Optical voltage mapping experiments of control and irradiated monolayers. (A, D) Conduction velocity (CV), (B, E) action potential duration at 50% repolarisation (APD_{50}), and (C, F) action potential duration at 90% repolarization (APD_{90}) of control (Ctrl) and irradiated monolayers 24h (A-C) or 96h (D-F) after irradiation (Rx) (Ctrl, *n*=5 and 6, resepctively; Rx, *n*=6) (G- H: Video Analysis of beating frequency using the Macro Myocyter for ImageJ with (G) representative contraction curves of a control and an irradiated cardiomyocyte 96h after Rx and (H) analysis of beating frequency before Rx (Ctrl *n*=6; Rx, *n*=8), 24h after Rx (*n*=6, each) and 96h after Rx (Ctrl *n*=8; Rx, *n*=7). Data are shown as box and whisker plots. (*p<0.05, **p<0.01, ***p<0.001, ****p<0.0001).

Fig.2: Radiation-induced ion channel remodeling 24 and 96h after Rx. (A) mRNA transcripts of ion channels of the ventricular action potential 24 and 96h after Rx (*n*=6, each). Representative western blots of ion channels 96 h after Rx compared to Ctrl and corresponding analysis of optical density are shown (*n*=6, each; B and C). Data are represented as box and whisker plots. (*p<0.05, **p<0.01, ***p<0.001).

Fig.3: Irradiation increased cardiac cell-to-cell coupling. (A) RT-qPCRs 24 and 96h after Rx (*n*=12, each). Western blot results 24 (B) and 96h after Rx (C) (*n*=6, each). (D) Quantification of the Cx43-area occupied relative to the membrane contact area 96h after Rx (Ctrl, *n*=113; Rx *n*=115). (E) Representative immunofluorescent stainings of Cx43 (red), cTnT (green) and DAPI (blue). A white box indicates the

location of Cx43 at the membrane contact area between neighbouring cells (scale bar=25µm). (E) Representative FRAP experiments with control and irradiated monolayers 96h after Rx (SB=25µm). (F) Average time courses of FRAP and (G) analysis of percent recovery 96h after Rx (Ctrl, *n*=23*;* Rx, *n*=15). Data are shown as box and whisker plots. (*p<0.05, ***p<0.001, ****p<0.0001).

Fig.4: Calcium transient analysis 24 and 96h after Rx. (A) and (G): Representative traces of control (black) and irradiated monolayers (red) 24 (A) and 96h after Rx (G). Analysis of diastolic calcium, peak amplitude, time-to-peak (TTP), full duration at half maximum (FDHM) and decay 24h after Rx (Ctrl, *n*=31*;* Rx, *n*=37). Analysis of diastolic calcium, peak amplitude, TTP, FDHM and decay 96h after Rx (Ctrl, *n*=39*;* Rx, *n*=52). Data are shown as box and whisker plots. (*p<0.05, **p<0.01, ***p<0.001, ****p<0.0001).

Fig.5: RT-qPCR and western blotting results of calcium handling proteins. (A) Changes in the mRNA transcripts of RYR2, SERCA (Atp2a1), NCX (Slc8a1), PLN and CaMKIId and CaMKIIγ at 24 and at 96h after Rx (n=6, each). (B) Western blotting of NCX and PLN 96h after Rx (n=6, each). (C) Western blotting of CaMKIIδ and CaMKIIγ 96 h after Rx (n=6, each). Data are shown as box and whisker plots. (*p<0.05, **p<0.01, ***p<0.001).

Fig.6: Irradiation did not affect structural features of cardiac fibroblasts in mixed cardiomyocyte and fibroblast cultures. Western blotting of α-SMA and vimentin (Vim) 96h after Rx with respective blots shown and analysis of optical density (n=6, each). Data are shown as box and whisker plots relative to Ctrl.

Supplemental Material

Cardiac stereotactic body radiotherapy to treat malignant ventricular arrhythmias directly affects the cardiomyocyte electrophysiology

Authors: Christine Mages, MD [a,b,c,d#], Heike Gampp [a,b#], Ann-Kathrin Rahm, MD [a,b,c,d], Juline Hackbarth [a,b], Julia Pfeiffer [a,b], Finn Petersenn [a,b], Xenia Kramp [a,b], Fatemeh Kermani [e], Juan Zhang, PhD [f], Daniel Pijnappels, PhD [f], Antoine A. F de Vries, PhD [f], Katharina Seidensaal, MD [g,h], Bernhard Rhein, PhD [g,h], Jürgen Debus, MD [g,h], Nina D. Ullrich, PhD [c,e,i], Norbert Frey, MD [a,b,c,d], Dierk Thomas, MD [a,b,c], Patrick Lugenbiel, MD [a,b,c*]

[a]Department of Cardiology, University Hospital Heidelberg, Heidelberg, Germany;

[b]Heidelberg Center for Heart Rhythm Disorders (HCR), University Hospital Heidelberg, Heidelberg, Germany;

[c]German Centre for Cardiovascular Research (DZHK), Partner site Heidelberg/Mannheim, University of Heidelberg, Heidelberg, Germany;

[d]Informatics4Life Consortium (Institute for Informatics Heidelberg), Heidelberg, Germany;

[e]Division of Cardiovascular Physiology, Institute of Physiology and Pathophysiology, Heidelberg, Germany;

fDepartment of Cardiology, Leiden University Medical Center, Leiden, the Netherlands

[g]Department of Radiation Oncology, Heidelberg University Hospital, Heidelberg, Germany;

[h]Heidelberg Institute of Radiation Oncology (HIRO), Heidelberg, Germany;

[i]Department of Physiology, University of Bern, Switzerland

# authors contributed equally

***Address for correspondence:** Patrick Lugenbiel, MD, FEHRA; Department of Cardiology, Heidelberg University, Im Neuenheimer Feld 410, 69120 Heidelberg, Germany; Tel.: ++49 6221 568855; Fax: ++49 6221 565514; E-Mail: patrick.lugenbiel@med.uni-heidelberg.de

Supplemental Methods

Isolation of Neonatal Rat Ventricular Cardiomyocytes (NRVCs) and Cell Culture

Primary cardiomyocytes were isolated from the hearts of 1- to 3-day old neonatal Wistar rats. Animal housing conditions and experimental procedures were performed in compliance with the German Law for the Protection and Use of Laboratory Animals. Rats were decapitated and the hearts dissected and washed in ice-cold Hank's balanced salt solution. Atria and large vessels were removed, ventricles were cut into small pieces and digested using DNAse II (Sigma-Aldrich, St. Louis, MO) and trypsin (Thermo Fisher Scientific, Waltham, MA), performing eight 10-min digestion steps at 37°C. The supernatant was collected in fetal bovine serum (FBS) after each step, pooled and centrifuged to separate the cells from remaining pieces of tissue. The cells were then resuspended in Dulbecco's modified Eagle medium (DMEM/F-12; 11039, Thermo Fisher Scientific) supplemented with 10% FBS (10270, Thermo Fisher Scientific), 1% penicillin/streptomycin (15140122, Thermo Fisher Scientific) and 1× L-glutamine (25030024, Thermo Fisher Scientific). A two-layer Percoll gradient was used to separate non-cardiomyocytes from cardiomyocytes. Collected cells were passed through a cell strainer (40µm, BD Falcon, Franklin Lakes, NJ) and then seeded into wells of 6-well cell culture plates (Thermo Fisher Scientific) coated with 0.02% gelatine (Thermo Fisher Scientific). For fluorescence recovery after photobleaching (FRAP), patch clamp and calcium transient experiments, cells were seeded on glass-

bottom dishes (Mattek, Ashland, OR) coated with 0.02% gelatine. The NRVCs were cultured in supplemented DMEM/F-12 as mentioned above at 37°C in 95% humidified air with 5% CO2. NRVCs showed spontaneous contraction after 24h in culture, at which time point the culture medium was replaced with fresh supplemented DMEM/F-12. NRVCs were cultured for a total of 6 days.

Photon Irradiation

NRVCs were subjected to 20Gy single-fraction photon irradiation on day 2 of cell culture using a biological cabinet X-ray irradiator X-RAD 320 (Precision X-Ray, North Branford, CT) at 320 keV and a dose rate of 500 cGy/min.

Optical Voltage Mapping

To assess the dynamics of action potential propagation in NRVC monolayers, optical mapping experiments were conducted. Using a fast and highly sensitive camera system MICAM Ultima - L (SciMedia USA, Costa Mesa, CA) and BrainVision Analyzer version 16.04.20 software (Brainvision, Tokyo, Japan), the propagation of electrical action potential in the cell cultures was recorded, visualized and analyzed. Cells were seeded in gelatin-coated 6-well plates at a density of 10^6 cells/well. The monolayers were incubated with 8µM of the voltage-sensitive fluorescent dye di-4-ANEPPS (D1199, Thermo Fisher Scientific) in DMEM/F-12 for 10 min in an incubator at 37°C, 5% CO_2 and 95% humidified air. Then, fresh DMEM/F-12 medium was applied, and the cells were placed on a constant heating plate at 37°C for the duration of the experiments.

Action potential light (λex = 525 ± 25nm) was emitted from a halogen arc lamp and delivered to the monolayers via epi-illumination. The fluorescent emission light (λem >590nm) was first passed through a diverging lens (1× Plan-Apo, WD=61.5mm; Leica, Wetzlar, Germany) and then a dichroic mirror and eventually focused on a 100×100 pixels complementary metal oxide semiconductor camera (MiCAM05-Ultima, SciMedia) through a 2× converging lens. The cells were electrically stimulated for the experiments at a frequency of 1Hz with an epoxy resin-coated bipolar platinum electrode (pulse strength 8V, pulse duration 10ms). The electrode was connected to a stimulus generator STG 2004 (Multi Channel Systems, Reutlingen, Germany) controlled by the software MC Stimulus II (v3.5.0, Multi-Channel Systems). The signals were acquired at a spatial resolution of 205 µm/pixel. The velocity of propagation and action potential characteristics were recorded during electrical stimulation at 1Hz. Signals were averaged with those from the 8 nearest pixels to minimize noise artefacts. The conduction velocity was analyzed, and action potential duration (APD) was calculated at 50% (APD_{50}) and 90% (APD_{90}) of repolarization. Statistical analysis was performed using GraphPad Prism 6 software (GraphPad Software, San Diego, CA).

Video Analysis of Beat Frequency

Beat frequency in recorded videos of cardiomyocytes was measured using the recently developed macro Myocyter (version 1.0), an analytical software tool for the ImageJ (version 1.52b) image processing software.[1] By scaling the time-dependent changes in pixel intensity in successive video images of recorded cardiomyocytes, Myocyter allowed visualization of cellular contractility. Spontaneous contractions of neonatal cardiomyocytes were recorded using an iPhone XR (Apple, Cupertino, CA)

connected to the eyepiece of a Leica DMi1 microscope via a camera adapter (Bresser, Rhede, Germany). Video recordings were done at 60 frames/s for 10-15s. Data extraction with Myocyter was performed according to the developer's instructions and beat frequency was analyzed using ImageJ 1.50i.[2]

RNA Isolation and Reverse Transcription Quantitative Real-Time PCR (RT-qPCR)

RNA isolation and RT-qPCR were performed as published elsewhere.[3] Briefly, RNA was isolated using QIAZol Lysis Reagent (Qiagen, Hilden, Germany) according to the manufacturer's instructions. RNA concentration was determined using a NanoDrop 2000/2000c spectrophotometer (Thermo Fisher Scientific) at a wavelength of λ=260 nm. The isolated RNA (3µg) was converted into DNA using the Maxima First Strand cDNA Synthesis Kit for RT-qPCR (Thermo Fisher Scientific) according to the manufacturer´s instructions. RT-qPCR was performed using the StepOnePlus PCR System (Thermo Fisher Scientific) and TaqMan Gene Expression Assay primers (Applied Biosystems, Foster City, CA; see Supplemental Table 1). Normalization was done using primers and probes for the housekeeping enzyme glyceraldehyde-3-phosphate dehydrogenase (GAPDH) using delta-delta-Ct method. All RT-qPCR reactions were performed in triplicate or a higher number of replicates, and a non-template control and dilution series were included on each plate for quantification. Data are expressed as the average of triplicates. All measurements were adjusted using a standard probe, and quantification was corrected for the amplification efficiency derived from the standard curves.

Protein Isolation and Western Blot Analysis

Proteins were extracted from NRVC and protein immunodetection was performed by sodium dodecyl sulfate (SDS)-polyacrylamide (PAA) gel electrophoresis and western blotting as previously reported.[3] Proteins were extracted in 20mM Tris-HCl, 0.5% Nonidet P-40, 0.5% sodium deoxycholate, 150mM NaCl, 1 mM EDTA, 1mM Na_3VO_4, 1mM NaF and inhibitors of proteases (cOmplete, Mini Protease Inhibitor Cocktail; Roche Applied Science, Indianapolis, IN). The resulting samples were centrifuged at 4°C for 30 min and 14,000×*g*, and the protein concentration in the supernatants was determined by the bicinchoninic acid protein assay (Thermo Fisher Scientific). Equal amounts of total protein were separated on SDS- 7.5-15% PAA gels and transferred to nitrocellulose membranes for 2h at 200mV (Amersham Protran 0.45 NC; GE Healthcare Life Sciences, Freiburg, Germany). After blocking in PBST containing 5% non-fat milk for 2h at room temperature (RT), membranes were incubated overnight with the primary antibodies listed in Supplemental Table 2. Next, the membranes were incubated with matching horseradish peroxidase (HRP)-conjugated goat anti-rabbit secondary antibody (ab6802, Abcam, Cambridge, United Kingdom), HRP- conjugated goat anti-mouse IgG (H+L) secondary antibody (1031-05, Southern Biotech, Birmingham, AL) or HRP-conjugated goat anti-mouse IgG1 cross-adsorbed secondary antibody (A10551, Thermo Fisher Scientific,). Signals were developed with the enhanced chemiluminescence detection reagent (ECL Western blotting Reagents; GE Healthcare, Buckinghamshire, United Kingdom). GAPDH was used as an internal control. Quantification of optical density was performed with ImageJ 1.50i software.

FRAP

FRAP was assessed as an indicator of gap junctional coupling efficiency. Photobleaching and imaging were performed on an Olympus FluoView confocal laser scanning microscopy (Olympus Corporation, Tokyo, Japan) using a 60× water immersion objective (1.2 NA). NRVC monolayers seeded on glass-bottom dishes were incubated for 20 min in the dark with 500µl of 0.5µM calcein-AM (Thermo Fisher Scientific) in Tyrode's solution. Calcein-AM was converted to green fluorescent calcein by intracellular esterases. After de-esterification, cells were washed with prewarmed Tyrode's solution for 10 min. Afterwards, the dye was no longer able to diffuse through the plasma membrane and could only leave cells through gap junctions. One cardiomyocyte within a monolayer was bleached with a laser power of 50% at 10 µs/pixel for 5s. Calcein diffusion from neighbouring cells into the bleached cell was measured over time and recovery of fluorescence was recorded in 50 images taken every 10s with a laser power of 0.5% at 2µs/pixel. Analysis was done in ImageJ to plot the time course of fluorescence recovery. After subtraction of background fluorescence and bleaching area, the plot was normalized to the fluorescence intensity before bleaching. Parameters were analysed using OriginLab software (OriginLab Corporation, Northampton, MA) and ImageJ 1.50i software.

Immunofluorescence Analysis

NRVCs on 20×20mm glass coverslips were washed with cold phosphate-buffered saline (PBS) for three times, fixed with 4% paraformaldehyde solution in PBS (Roti-Histofix, Carl Roth, Karlsruhe, Germany) for 10 min at RT. Cells were permeabilized with PBS containing 0.1% Triton X-100 (Merck, Darmstadt, Germany) for 3 min, followed by a blocking step with 5% Gibco normal goat serum (Thermo Fisher

Scientific) and 0.1% Triton X-100 in PBS for 2h. Cells were incubated overnight with the following primary antibodies: rabbit polyclonal to connexin 43 (Cx43), mouse monoclonal to cardiac troponin T (cTnT), rabbit polyclonal to cTnT and mouse monoclonal to vimentin. Next, cells were incubated with matching secondary antibodies conjugated to Alexa Fluor dyes with different excitation-emission spectra for 2h at RT and protected from light, using Alexa Fluor 568-conjugated donkey-anti-rabbit IgG (H+L) (A11057, diluted 1:1000; Thermo Fisher Scientific) or Alexa Fluor 488-conjugated goat-anti-mouse IgG (H+L) (A32723; diluted 1:1000, Thermo Fisher Scientific). All antibodies were diluted in blocking buffer. Cells were mounted with Fluoroshield (Sigma-Aldrich containing DAPI (4`,6-diamidino-2-phenylindol dihydrochloride (Abcam) for nuclear staining. Laser-scanning confocal imaging was used to estimate the expression of Cx43. Images were taken on a Leica SP8 confocal microscope with a 63× oil immersion objective and analyzed using the ImageJ 1.50i software. All immunofluorescence images were taken at the same light intensity and photodetector setting to ensure a fair comparison. Cell surface Cx43 levels were expressed as the ratio of the area of Cx43 plaque to the intercellular border area.

Calcium Transient Measurements

Calcium transients of NRVCs were measured with the calcium- sensitive fluorescent dye fura-2-AM (Thermo Fisher Scientific). NRVCs seeded on glass-bottom dishes were loaded with 1.5μM of fura-2-AM in Tyrode's solution and incubated for 20 min, followed by washing with Tyrode's solution and waiting 10 min for de-esterification. Cells were continuously perfused with pre-heated Tyrode's solution containing Probenecid (100μM; Sigma Aldrich) to prevent secretion of fura-2. Calcium transients were recorded using an IonOptix system (IonOptix, Dublin, Ireland). NRVCs were

exposed to light from a xenon lamp passing through fast-switching filters of 340nm and 380nm to determine the ratio of bound and unbound calcium ions in the cells. Fluorescence emission light was collected at 510nm. Data are presented as fura-2 ratio (F340/F380nm) and collected using the IonWizard software developed by IonOptix. Three representative calcium transients were analysed per recording using OriginPro software. Assessed parameters comprised diastolic calcium level, amplitude, time-to-peak, full duration at half maximum and decay. Decay of calcium transients was calculated using an exponential decay function.

Terminal Deoxynucleotidyl Transferase dUTP Nick End Labeling (TUNEL) Staining

TUNEL staining was performed using the In Situ Cell Death Detection Kit, TMR red of Roche Applied Science according to the manufacturer's protocol. Cells on glass coverslips were washed three times with PBS and then fixed with 4% buffered paraformaldehyde for 10 min. After another washing step, the cells were permeabilized by incubation with 0.1% Triton- X100 in PBS for 2 min at 4°C. The positive control consisted of permeabilized cells treated for 10 min at RT with recombinant DNase I (3U/ml in 50 mM Tris-HCl (pH 7.5); Roche, Mannheim, Germany), 1mg/ml bovine serum albumin) to induce double-strand breaks. Next, 5µl Enzyme Solution and 45µl Label Solution were mixed and added to each coverslip. Instead of the reaction mix, 50µl Label Solution was added to the negative control sample. After incubation for 1h in a humidified dark chamber at 37°C, the coverslips were washing three times with PBS covered with antifade containing For immunofluorescent stainings evaluating the proportion of cardiomyocytes and

fibroblasts in culture, imaging was performed with an inverted Axio Observer Z1 microscope and an Axiocam 506 camera (Carl Zeiss) Cells were labelled with rabbit polyclonal anti-troponin T antibodies to identify (cardiomyocytes and mouse monoclonal anti-vimentin antibodies to mark cardiac fibroblasts. Secondary antibodies were Alexa Fluor 568-conjugated donkey-anti-rabbit (A11057, diluted 1:1000; Thermo Fisher Scientific) and Alexa Fluor 488-conjugated goat-anti-mouse (A32723; diluted 1:1000, Thermo Fisher).

Immunofluorescence analysis of cell culture was performed with an inverted Axio Observer Z1 microscope (Carl Zeiss, Jena, Germany) and an Axiocam 506 camera (Carl Zeiss). TUNEL-positive cells were counted manually, and ImageJ 1.41 software was used to calculate the total cell number in 3×3 tiles. Excitation wavelengths in the range of 520-560nm (maximum 540nm; green) were used as well as detection wavelengths in the range of 570-620nm (maximum 580nm, red). The percentage of TUNEL-positive cells was calculated by dividing TUNEL-positive cells by total cell count.

Patch Clamp Recordings of Action Potentials

For action potential recordings, NRVCs were cultured on 35mm glass-bottom dishes at single cell density. Measurements were performed in whole-cell patch-clamp configuration using a HEKA EPC-10 patch clamp amplifier (HEKA Instruments, Holliston, MA) connected to an inverted Olympus IX81 FluoView1000confocal laser scanning microscope (Olympus, Tokyo, Japan) as previously described.[2] Data were acquired using PatchMaster (HEKA Instruments). Glass pipettes were pulled from borosilicate glass capillaries (GB150-8P; Science Products Hofheim am Taunus, Germany) using a DMZ Universal Puller (Zeitz Instruments, Martinsried, Germany) to

achieve pipette resistances of 1.5 - 2.5MΩ. The intracellular solution consisted of 120 mM KCl, 10mM HEPES, 5mM $MgCl_2$, 5 mM EGTA, 2.5mM Na_2-ATP, and the pH was adjusted to 7.2 using KOH. The external solution contained normal Tyrode (140mM NaCl, 6mM KCl, 1.8mM $CaCl_2$, 1.1mM $MgCl_2$, 10mM D-glucose, 10mM HEPES) and the pH was adjusted to 7.4 using NaOH. To determine the action potential stimulation threshold, a series of stepwise increasing stimulation currents (ranging from 100pA to 500nA with a step size of 100pA) was delivered. The first current resulting in an amplitude above the threshold was used to trigger action potentials. Action potential parameters were analyzed using OriginPro software.

Supplemental Figures and tables

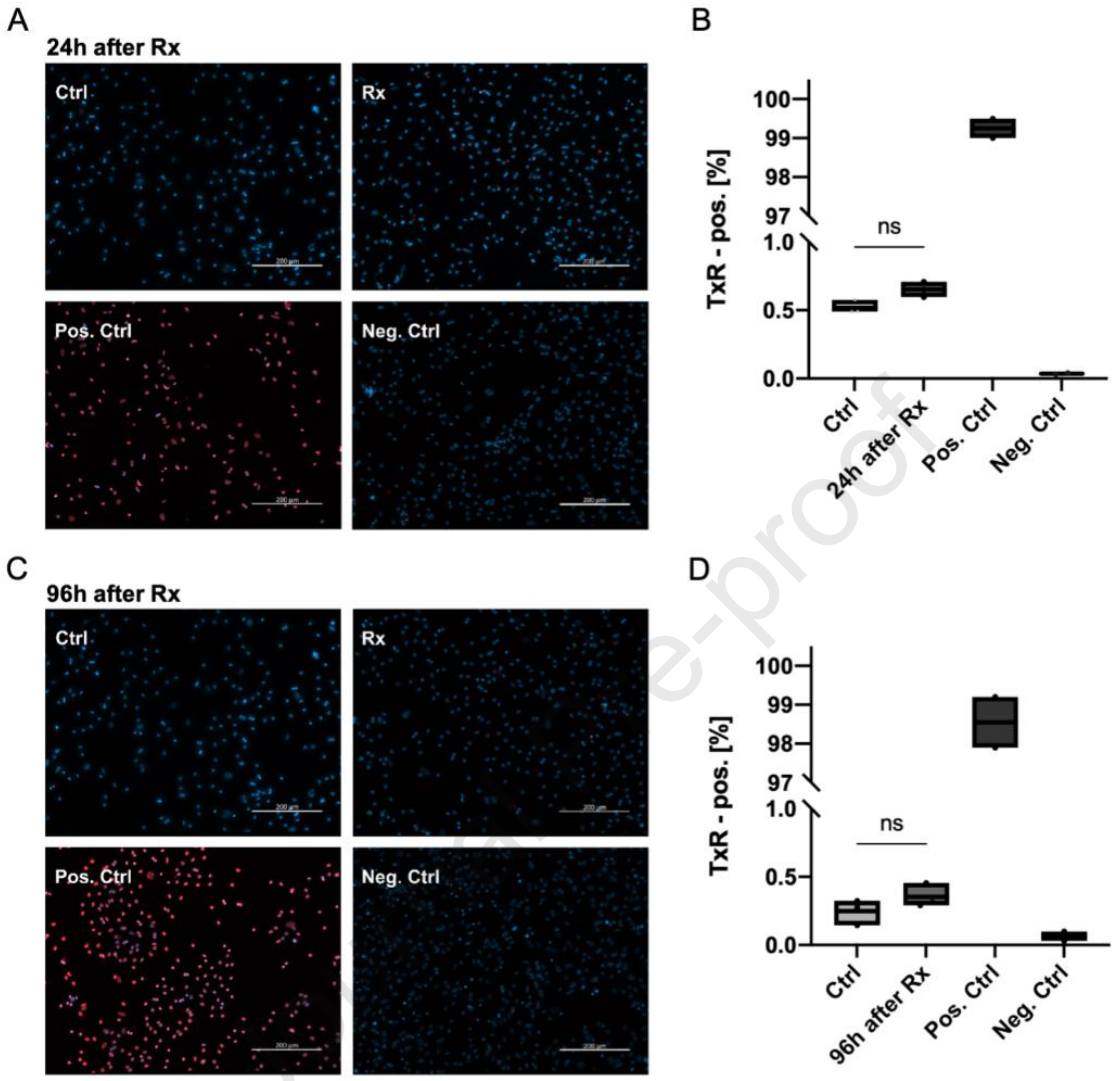

Supplemental Figure 1: Irradiation did not impact apoptosis rate in NRVCs. Representative fluorescence stainings of TUNEL assays (scale bar, 100µm) at (A) 24h and (C) 96h after radiation (Rx). Red nuclear fluorescence reflects endonucleolytic DNA degradation and apoptosis. Mean apoptosis rates at (B) 24h (*n=3,* each) and (D) 96h after Rx (*n=3,* each). TUNEL (Texas Red, TxR)-positive cells are expressed in relation to the total number of cells. Data are shown as box and whisker plots. Ctrl, control.

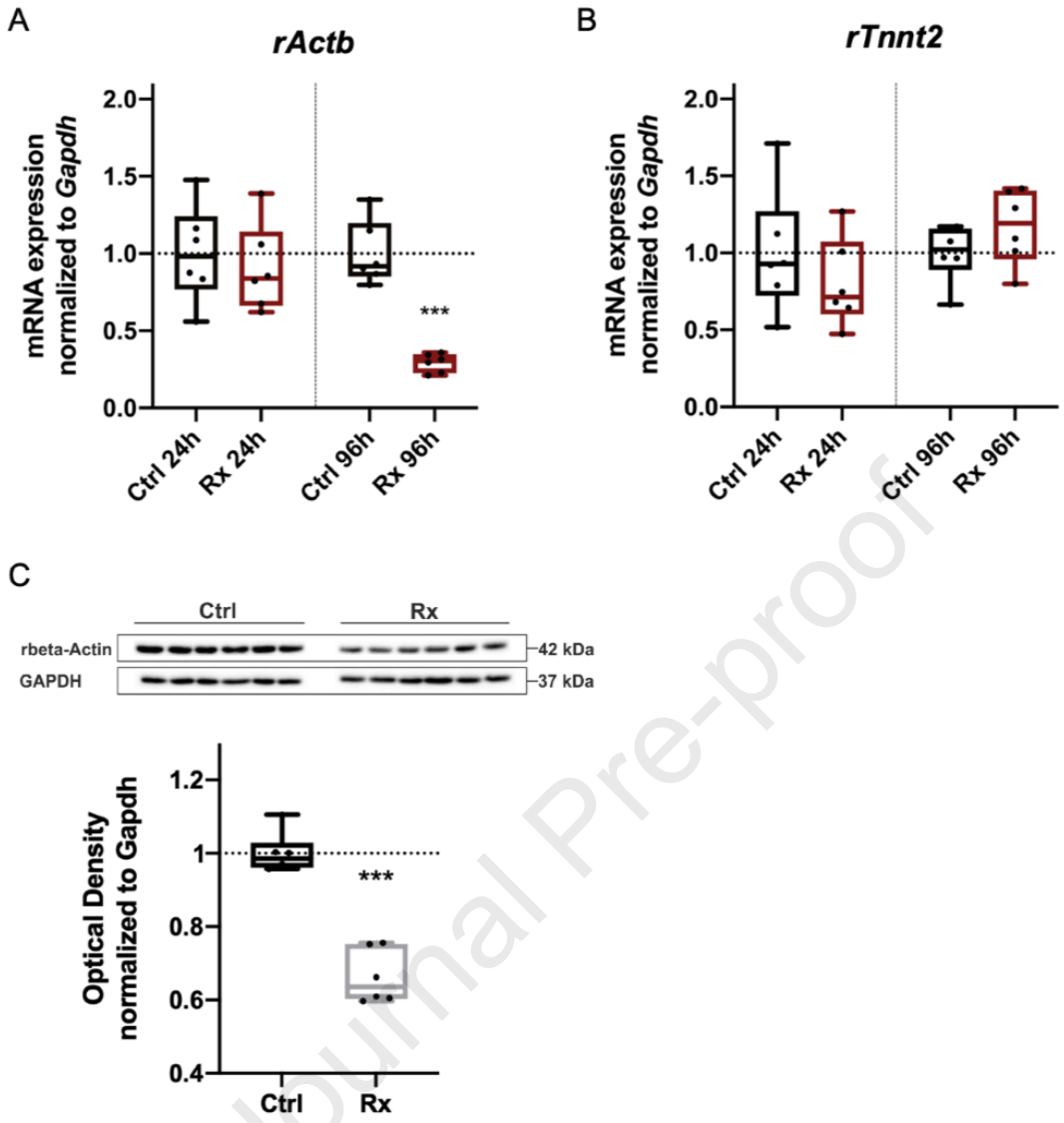

277

278 **Supplemental Figure 2: Structural changes after irradiation.** RT-qPCR analysis of
279 (A) *Actb* mRNA (*n=6*, each). and (B) *Tnnt2* mRNA (*n=6*, each) levels in irradiated (Rx)
280 and non-irradiated (Ctrl) NRVCs. (C) Western blot analysis of beta-actin protein levels
281 (*n*=6, each) in irradiated and Ctrl NRVCs. Data are shown as box and whisker plots.
282 (*p<0.05, **p<0.01, ***p<0.001).

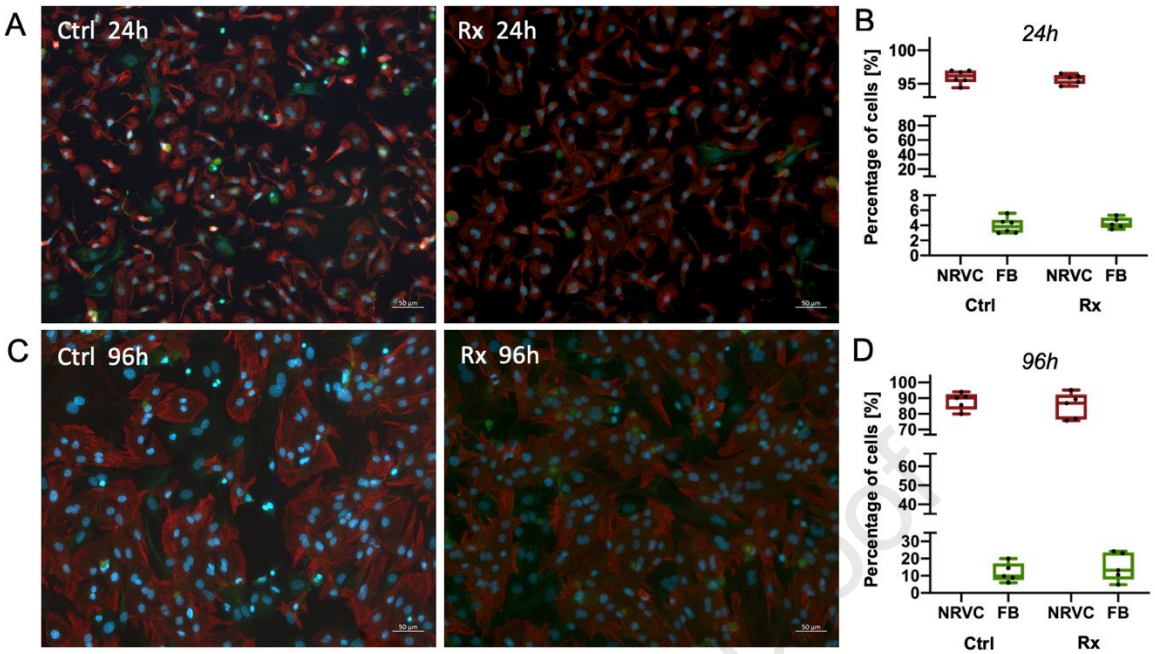

283

284 **Supplemental Figure 3: NRVC to cardiac fibroblast ratio at 24h and 96h after**
285 **irradiation.** Representative stainings of cardiomyocytes (red, cTNT) and fibroblasts
286 (green, vimentin) (A) 24h and (C) 96h after irradiation (Rx). Analysis of the ratio of
287 cells in culture (B) 24h after Rx (Ctrl: *n*=5, Rx: *n*=6) and (D) 96h after Rx (*n*=5, each*)*.
288 Data are shown as box and whisker plots. Ctrl, control.

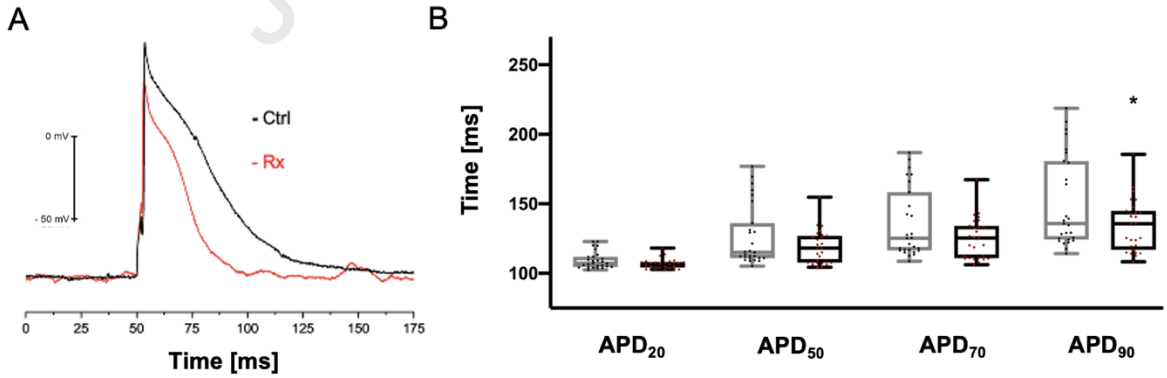

289

290 **Supplemental Figure 4: Action potential characteristics of control and irradiated**
291 **cardiomyocytes 24h after Rx.** (A): Representative traces of ventricular action
292 potentials of control cardiomyocytes (black) and irradiated cardiomyocytes (red) at 24h

after Rx. (B): Analysis of resting membrane potential (RMP), action potential amplitude (APA) and action potential duration at 20%, 50%, 70% and 90% repolarization (APD_{20}, APD_{50}, APD_{70}, APD_{90}), *n*=27, each. Data are shown as box and whisker plots. (*p<0.05).

Supplemental Table 1: PCR primers sorted alphabetically

Primer	ThermoFisher Catalogue Number	Chromosome Location
rActb	Rn00667869_m1	Chr.12: 13715843 - 13718813 on Build Rnor_6.0
rAtp2a1	Rn01508014_m1	Chr.1: 197855912 - 197875038 on Build Rnor_6.0
rCacna1c	Rn00709287_m1	Chr.4: 150639043 - 151269159 on Build Rnor_6.0
rCamkIIδ	Rn00560913_m1	Chr.2: 230900907 - 231130336 on Build Rnor_6.0
rCamkIIγ	Rn01537033_m1	Chr.15: 3936714 - 3995740 on Build Rnor_6.0
rGapdh	Rn01775763_g1	Chr.4: 157676396 - 157680271 on Build Rnor_6.0
rGja1	Rn06415115_s1	Chr.20: 37876589 - 37889097 on Build Rnor_6.0

rKcnd3	Rn04339184_m1	Chr.2: 207923775 - 208140727 on Build Rnor_6.0
rKcne1	Rn01767120_m1	Chr.11: 32498260 - 32508420 on Build Rnor_6.0
rKcnh2	Rn01442522_m1	Chr.4: 7355161 - 7387243 on Build Rnor_6.0
rKcnj12	Rn02533449_s1	Chr.10: 47282208 - 47343501 on Build Rnor_6.0
rKcnj2	Rn00568808_s1	Chr.10: 99429265 - 99442520 on Build Rnor_6.0
rKcnj8	Rn01492857_m1	Chr.4: 176783287 - 176789143 on Build Rnor_6.0
rKcnk2	Rn00597042_m1	Chr.13: 107690111 - 107886476 on Build Rnor_6.0
rKcnk3	Rn04223042_m1	Chr.6: 27154274 - 27190209 on Build Rnor_6.0
rKcnq1	Rn00583376_m1	Chr.1: 216293087 - 216630339 on Build Rnor_6.0
rPln	Rn01434045_m1	Chr.20: 34633157 - 34642904 on Build Rnor_6.0
rRyr2	Rn01470303_m1	Chr.17: 65533998 - 65955606 on Build Rnor_6.0
rScn5a	Rn00565502_m1	Chr.8: 128169191 - 128266639 on Build Rnor_6.0

rSlc8a1	Rn04338914_m1	Chr.6: 4245582 - 4564263 on Build Rnor_6.0
rTnnt2	Rn00562059_m1	Chr.13: 52662973 - 52680992 on Build Rnor_6.0

299

300 **Supplemental Table 2**: Western blotting antibodies sorted alphabetically.

Primary Antibody	Class	Host	Dilution	Company
Anti-alpha-smooth-muscle-actin (14-9760-82)	monoclonal	mouse	1:1000	Invitrogen, Thermo Fisher Scientific
Anti-beta actin antibody (ab8227)	polyclonal	rabbit	1:3000	Abcam
Anti-CaMKII delta antibody (ab181052)	polyclonal	rabbit	1:1000	Abcam
Anti-CaMKII gamma antibody (ab262701)	polyclonal	rabbit	1:1000	Abcam
Anti-Cav1.2 (CACNA1C) antibody (MA5-27717)	monoclonal	mouse	1:1000	Invitrogen, Thermo Fisher Scientific
Anti-Cx43 antibody (ab11370)	polyclonal	rabbit	1:3000	Abcam
Anti-GAPDH antibody (ab181602)	polyclonal	rabbit	1:10000	Abcam

Anti-KCNK2/TREK-1 antibody (APC-047)	polyclonal	rabbit	1:1000	Abcam
Anti-Kir2.1 (KCNJ2) antibody (APC-026)	polyclonal	rabbit	1:1000	Abcam
Anti-Kir6.1 (KCNJ8) antibody (ab241996)	monoclonal	mouse	1:1000	Abcam
Anti-Kv11.1 (KCNH2) antibody (APC-062)	polyclonal	rabbit	1:1000	Abcam
Anti-Kv4.3 (KCND3) antibody (APC-017)	polyclonal	rabbit	1:1000	Abcam
Anti-Kv7.1 (KCNQ1) antibody (MA5-27676)	monoclonal	mouse	1:1000	Invitrogen, Thermo Fisher Scientific
Anti-$Na_v1.5$ (SCN5A) (493-511) antibody (ASC-005)	polyclonal	rabbit	1:500	Almone Labs
Anti-NCX (SLC8A1) antibody (ASC-005)	polyclonal	rabbit	1:1000	Alomone Labs
Anti-Phospholamban (PLN) (MA3-922)	monoclonal	mouse	1:1000	Invitrogen, Thermo Fisher Scientific
Anti- Vimentin (VIM) antibody (ab8069)	monoclonal	mouse	1:1000	Abcam

301

302

Supplemental references

1. Rasband, W.S., ImageJ, U. S. National Institutes of Health, Bethesda, MA, https://imagej.net/ij/, 1997-2018.

2. Grune T, Ott C, Häseli S, Höhn A, Jung T. The “MYOCYTER” – Convert cellular and cardiac contractions into numbers with ImageJ. Sci Rep. 2019;9:15112.

3. Syren P, Rahm A-K, Schweizer PA, et al. Histone deacetylase 2-dependent ventricular electrical remodeling in a porcine model of early heart failure. Life Sci. 2021;281:119769.